NAVAL
POSTGRADUATE
SCHOOL

MONTEREY, CALIFORNIA

THESIS

VISIBILITY OVER LAND FROM CONTRAST ANALYSIS OF MULTI-SPECTRAL SATELLITE OBSERVATIONS

by

Dominick A. Vincent

September 2003

Thesis Advisor:	Philip A. Durkee
Second Reader:	Carlyle H. Wash

Approved for public release; distribution is unlimited.

THIS PAGE INTENTIONALLY LEFT BLANK

REPORT DOCUMENTATION PAGE			Form Approved OMB No. 0704-0188

1. AGENCY USE ONLY *(Leave blank)*	2. REPORT DATE September 2003	3. REPORT TYPE AND DATES COVERED Master's Thesis

4. TITLE AND SUBTITLE: Visibility Over Land from Contrast Analysis of Multi-Spectral Satellite	5. FUNDING NUMBERS
6. AUTHOR(S) Dominick A. Vincent	
7. PERFORMING ORGANIZATION NAME(S) AND ADDRESS(ES) Naval Postgraduate School Monterey, CA 93943-5000	8. PERFORMING ORGANIZATION REPORT NUMBER
9. SPONSORING /MONITORING AGENCY NAME(S) AND ADDRESS(ES) N/A	10. SPONSORING/MONITORING AGENCY REPORT NUMBER

11. SUPPLEMENTARY NOTES The views expressed in this thesis are those of the author and do not reflect the official policy or position of the Department of Defense or the U.S. Government.

12a. DISTRIBUTION / AVAILABILITY STATEMENT Approved for public release; distribution is unlimited.	12b. DISTRIBUTION CODE

13. ABSTRACT ***(maximum 200 words)***

The objective of this thesis is to investigate the viability of using contrast reduction in multi-spectral satellite observations to characterize surface visibility reduction due to heavy aerosol loading. Two methods are explored. First, the spectral distribution of standard deviation of surface reflectance over a homogeneous background (urban, agriculture, or forested) is plotted for three aerosol conditions (dust, smoke, and low aerosol loading). Second, the same cases are analyzed using a pixel-to-pixel differencing of surface reflectance. The spectral distributions of the means for the resulting difference fields are constructed. Each aerosol type was found to exhibit a relatively unique spectral distribution for both methods. Each background was found to exhibit a characteristic amount of contrast in the absence of heavy aerosol loading. The unique spectral characteristics for each aerosol-background combination may be correlated to aerosol optical depths or surface visibilities with corrections for sensor view angle variations, Rayleigh scattering, and masking of clouds and surface water. The spectral distribution-aerosol optical depth correlation can be used to build an empirical model for aerosol optical depth and surface visibility retrievals from satellite observations. This method may be applied to multi-spectral or panchromatic imagery, unlike current aerosol optical depth retrievals over land.

14. SUBJECT TERMS Aerosol, Satellite Observations, Aerosol Optical Depth Retrieval, Over Land, Contrast	15. NUMBER OF PAGES 69
	16. PRICE CODE

17. SECURITY CLASSIFICATION OF REPORT	18. SECURITY CLASSIFICATION OF THIS PAGE	19. SECURITY CLASSIFICATION OF ABSTRACT	20. LIMITATION OF ABSTRACT
Unclassified	Unclassified	Unclassified	UL

NSN 7540-01-280-5500

Standard Form 298 (Rev. 2-89)
Prescribed by ANSI Std. 239-18

THIS PAGE INTENTIONALLY LEFT BLANK

Approved for public release; distribution is unlimited.

VISIBILITY OVER LAND FROM CONTRAST ANALYSIS OF MULTI-SPECTRAL SATELLITE OBSERVATIONS

Dominick A. Vincent
Lieutenant Commander, United States Navy
B.S., Texas A&M University, 1994

Submitted in partial fulfillment of the
requirements for the degree of

MASTER OF SCIENCE IN METEOROLOGY AND PHYSICAL OCEANOGRAPHY

from the

NAVAL POSTGRADUATE SCHOOL
SEPTEMBER 2003

Author: Dominick A. Vincent

Approved by: Philip A. Durkee
Thesis Advisor

Carlyle H. Wash
Second Reader and Chairman, Department of Meteorology

THIS PAGE INTENTIONALLY LEFT BLANK

ABSTRACT

The objective of this thesis is to investigate the viability of using contrast reduction in multi-spectral satellite observations to characterize surface visibility reduction due to heavy aerosol loading. Two methods are explored. First, the spectral distribution of standard deviation of surface reflectance over a homogeneous background (urban, agriculture, or forested) is plotted for three aerosol conditions (dust, smoke, and low aerosol loading). Second, the same cases are analyzed using a pixel-to-pixel differencing of surface reflectance. The spectral distributions of the means for the resulting difference fields are constructed. Each aerosol type was found to exhibit a relatively unique spectral distribution for both methods. Each background was found to exhibit a characteristic amount of contrast in the absence of heavy aerosol loading. The unique spectral characteristics for each aerosol-background combination may be correlated to aerosol optical depths or surface visibilities with corrections for sensor view angle variations, Rayleigh scattering, and masking of clouds and surface water. The spectral distribution-aerosol optical depth correlation can be used to build an empirical model for aerosol optical depth and surface visibility retrievals from satellite observations. This method may be applied to multi-spectral or panchromatic imagery, unlike current aerosol optical depth retrievals over land.

THIS PAGE INTENTIONALLY LEFT BLANK

TABLE OF CONTENTS

LIST OF FIGURES

THIS PAGE INTENTIONALLY LEFT BLANK

LIST OF TABLES

THIS PAGE INTENTIONALLY LEFT BLANK

ACKNOWLEDGMENTS

First, I would like to thank my advisor, Dr. Philip A. Durkee of the Department of Meteorology, Naval Postgraduate School, for his unwavering guidance, support, and patience during the thesis development process. I would also like to thank Dr. Carlyle H. Wash for his input as second reader. Together, they have pushed me to develop concepts that contribute to academia *and* the effectiveness of the warfighter.

I would like to thank Mr. Kurt Nielsen for his technical expertise and personal support through the many course changes during the thesis process. Without Kurt, I would still be staring at a blank computer screen. I would like to thank the members of my class, CDR Juan Aguilar (Mexican Navy), LCDR Victor Ross, Lt Cmdr. Andy Moys (Royal Navy), LCDR Claude Gahard, and LT Jeff Dixon, for their camaraderie during our time at NPS. I would also like to thank LCDR Dan Eleuterio for his support during both the education process and the PhD selection process.

Finally, I would like to thank my family, my wife, Gwen, my daughter, Marissa, and my son, Connor. Without their love, support, and understanding, none of this would have been possible. With all my love, I dedicate my work to them.

THIS PAGE INTENTIONALLY LEFT BLANK

I. INTRODUCTION

Atmospheric aerosols impact the Earth's energy budget through reflection and absorption of solar radiation (the aerosol direct effect) and modification of cloud properties (the aerosol indirect effect). The direct effect of aerosols works to scatter incoming solar radiation resulting in a net decrease in heating at the Earth's surface. The indirect effect works to increase cloud albedo at solar wavelengths by providing additional cloud condensation nuclei that produces more and smaller drops that result in brighter clouds. Again, this reduces heating at the Earth's surface. When compared to the global heating caused by anthropogenic greenhouse gases, cooling due to aerosols offsets greenhouse gas warming by approximately 25 to 50% (IPCC 2001, Twomey *et al.* 1984, Charlson *et al.* 1992, Kiehl and Briegleb 1993). Aerosols, however, are much harder to characterize and quantify than greenhouse gases. Greenhouse gases have a relatively homogeneous distribution globally and a lifetime of up to 100 years (ICCP 2001, Andreae *et al.* 1986). Aerosols have heterogeneous spatial and temporal distributions with life spans of approximately a week (ICCP 2001, Andreae *et al.* 1986). Recent research efforts, especially in the fields of remote sensing and modeling, have focused on characterizing the sources and distributions of natural and anthropogenic aerosols and distinguishing between the climatic effects of each.

Ideally, characterization of aerosol optical properties should be approached with a triad of observational techniques that include remote and *in situ* ground measurements, remote and *in situ* airborne measurements, and satellite observations. Ground measurements are provided by sun photometers, spectrometers, radiometers, and lidars. Their use, however, is limited spatially and temporally. Airborne measurements require instruments similar to those used in ground measurements with the addition of nephelometers and impactors capable of directly measuring aerosol size and concentration. Airborne measurements also provide the ability to determine the vertical distribution of aerosols. Again, however, airborne measurements are limited spatially and temporally, although less so than ground measurements. Satellite observations of aerosols are limited to radiometers and lidars but provide information on spatial distribution and source regions not available from point measurements. Improvements in

spatial and spectral resolution of radiometers found on current research satellites, such as Earth Observing System's Terra and Aqua satellites, can provide information unavailable from older satellite systems. An observational dataset that balances all three legs of the triad is difficult to find. Typically, such a dataset is only available from a large-scale field experiment requiring intricate planning and coordination and significant manpower. For this reason, satellite observations are widely used with ground and airborne measurements providing the validation data when available.

Characterization of aerosols is also important to the Department of Defense. The increasing reliance on the use of electro-optical weapons for precision strike has demanded an increased ability to quantify aerosol distributions both spatially and temporally. The areas of interest to the Department of Defense are often hostile, therefore *in situ* measurements, while preferred, are often unavailable. Much effort has been focused on aerosol characterization using satellite observations. Over water aerosol characterization efforts have met with much success. Over land efforts have proven much more difficult due to the complexity added by the variability of the land surface characteristics. Current satellite techniques for characterizing aerosols over land require large bodies of water or large areas of vegetation and are therefore highly background dependent. The Department of Defense, however, is often interested in areas where such limitations cannot be accommodated, such as desert regions. For this reason, alternative methods for characterizing aerosols over land using satellite observations must be explored.

One possible approach to characterizing and quantifying aerosols over land involves measuring the pixel-to-pixel contrast in regions of a satellite observation outside of clouds or in the absence of clouds. The amount of aerosol between the ground (background) and the sensor is inversely proportional to the contrast seen between pixels in the image. The reduced contrast seen in the presence of aerosol as compared to some low aerosol loading case, for the same area, can potentially be used to gauge the aerosol loading for that area.

The main objectives of this thesis are twofold:

1) Evaluate the potential of using a standard deviation method to determine pixel-to-pixel contrast reduction as a measure of aerosol presence and

properties against three different backgrounds; urban, agricultural, and forested areas, and

2) Evaluate the potential of using a differencing method to determine pixel-to-pixel contrast reduction as a measure of aerosol presence and properties against three different backgrounds; urban, agricultural, and forested areas.

Chapter II describes the background and previous approaches to over land aerosol characterization efforts. Chapter III describes the data sets and instrumentation used to collect the data. Chapter IV describe the two methods used evaluate contrast reduction in the satellite imagery. Chapter V presents the results and Chapter VI discusses final conclusions and recommendations.

THIS PAGE INTENTIONALLY LEFT BLANK

II. BACKGROUND

A. AEROSOL OPTICAL DEPTH RETRIEVALS

Atmospheric aerosols are a major source of uncertainty in the global heat budget due to the large spatial and temporal variability in sources, chemical composition, and microphysical properties. Aerosols may be either liquid or solid and may derive from natural or anthropogenic sources. One proposed strategy for global characterization of aerosol distribution and properties relies on a synergy between satellite analysis of aerosol spatial distribution over both land and ocean and continuous ground-based remote sensing and *in situ* measurements of aerosols from a global network of observation sites (Kaufman et al. 1997a, Prospero and Nees 1986). Aerosol retrievals over the ocean are routinely done over the low reflectance oceans that provide a dark background at the red-visible and near-infrared solar wavelengths. Aerosol retrievals over land are complicated by the heterogeneous reflective properties of the brighter land surface. Such retrievals are only successful when the "dark object" approach suggested by Kaufman and Sendra (1988) is used in areas where dense vegetation or large bodies of water are present. The method proposed here for aerosol optical depth retrieval over land uses reduction in apparent variability of the surface reflective properties to gauge the contrast reduction due to the intervening atmospheric aerosol.

B. OVER-WATER AEROSOL OPTICAL DEPTH RETRIEVALS

Current operational satellite optical depth retrievals are limited to reflectance measurements in the ocean environment. Retrievals are possible using reflectance measurements in one channel from a geostationary satellite (e.g., GOES) (Fraser et al. 1984, Knapp *et al.* 2002) or two channels from a polar orbiter (e.g., NOAA-AVHRR) (Kaufman *et al.* 1990, Durkee *et al.* 1991, Nakajima and Higurashi 1998, Mishchenko *et al.* 1999). According to Durkee *et al.* (1986), the satellite observed radiance in the visible and near-infrared wavelengths can be written as:

$$L = L_O \tau_O + L_{Rayleigh} + L_{aerosol}\,, \tag{2.1}$$

where L_O is the radiance leaving the surface, τ_O is the transmittance from the surface to the satellite, $L_{Rayleigh}$ is the radiance due to Rayleigh scattering by air molecules, and $L_{aerosol}$ is the radiance due to scattering by aerosols. The surface-leaving radiance, L_O, is greatly simplified over the ocean. However, surface glint due to specular ocean surface reflectance and reflectance by water constituents can enhance the surface-leaving radiance and mask that portion of the total signal attributed to aerosols. Such contributions can be avoided through the proper choice of sun-sensor geometry and avoiding areas of high concentrations of reflective ocean constituents. Radiance due to Rayleigh scattering is accounted for using model calculations (e.g. Kaufman 1979). The reflectance of the ocean in the red portion of the spectrum is less than 0.5% and near zero for wavelengths longer than 0.7 micrometers (Ramsey 1968). The remaining signal, in the absence of the contaminants mentioned above, is due to aerosol.

According to Kidder and Vonder Haar (1999), the radiative transfer equation can be written for the aerosol radiance, assuming only a single scatter, as:

$$\mu \frac{dL_{aerosol}}{d\delta_\lambda} = -L_{aerosol} + \frac{\tilde{\omega}_O}{4\pi} E_{sun} p(\psi_{sun}) \exp\left(-\frac{\delta_{aerosol} - \delta_\lambda}{\mu_{sun}} \right), \qquad (2.2)$$

where δ_λ is the vertical optical depth, $\delta_{aerosol}$ is the vertical aerosol optical depth of the entire atmosphere, and μ is the cosine of the satellite viewing angle. The solution to the first order, linear, ordinary differential equation is

$$L_{aerosol} = \frac{\tilde{\omega}_O}{4\pi} E_{sun} p(\psi_{sun}) \left(\frac{\mu_{sun}}{\mu_{sun} + \mu} \right) \left\{ 1 - \exp\left[-\delta_{aerosol} \left(\frac{\mu_{sun} + \mu}{\mu \mu_{sun}} \right) \right] \right\}. \qquad (2.3)$$

The aerosol optical depth is often much less than one. As such, the signal received at the satellite can be approximated as

$$L_{aerosol} = \frac{\tilde{\omega}_O}{4\pi} E_{sun} p(\psi_{sun}) \frac{\delta_{aerosol}}{\mu}. \qquad (2.4)$$

Equation 2.4 can be used to retrieve aerosol optical depth if the other terms of the right-hand side (RHS) are known. Irradiance from the sun, the solar zenith angle, and the satellite-viewing angle are all easily calculated. Irradiance from the sun, E_{sun}, is a function of the time of year, the solar spectrum, and the spectral response function of the satellite radiometer and can be easily calculated. The solar zenith angle is a function of

time and the location of the scan spot. The satellite-viewing angle is a function of the location of the satellite and that of the scan spot. The single-scatter albedo and the scattering phase function are a function of the index of refraction and the size distribution of the aerosols. As such, they require *a priori* knowledge of the aerosol's properties before the equation can be solved.

The over-water approach has several limitations. The algorithms based on this method must assume a model aerosol type and size distribution to determine the single-scatter albedo and the scattering phase function necessary to solve Eq. 2.4. The aerosol models used are typically those from literature that best represent the local conditions (Whitby 1978, Shettle and Fenn 1979, and D'Almeida *et al.* 1991). These model distributions can be assumed or be objectively chosen using a method developed by Durkee *et al.* (1991) in which the ratio between AVHRR channels 1 and 2 is used to select a model size distribution. Either method may be used with single channel geostationary satellite observations (Kuciauskus 2002). The two-channel method, however, lessens the uncertainty caused by assuming a single-scatter albedo and scattering phase function.

C. OVER-LAND AEROSOL OPTICAL DEPTH RETRIEVALS

Over land, the surface leaving radiance term in Eq. 2.1, L_O, cannot be simplified as in the case over the ocean. Surface reflectance over land can be quite variable depending on the background. The high surface reflectance can easily overwhelm that part of the signal due to aerosol, which is typically very optically thin. For this reason, aerosol retrievals are closely tied to surface characterization (Wen *et al.* 1999).

Initial efforts to retrieve aerosol optical depth over land in the presence of anthropogenic haze used a clear atmosphere case of the same area as a reference (Fraser *et al.* 1984, Kaufman *et al.* 1990, Ferrare *et al.* 1990). This assumes that surface reflectance will be consistent between cases. Kaufman and Sendra (1988) developed a "dark object" approach to over land aerosol optical depth retrievals that reduces surface effects in densely vegetated or forested regions. The dark object approach assumes that the low surface reflectance minimizes the error in the retrieved optical depth as compared

to errors over bright surfaces. The dark object approach also allows the use of the correlations between the middle-IR band at 2.2 micrometers and the blue and red bands in the visible. Thus, the middle-IR band may be used to estimate surface reflectance in these bands and infer optical depths in both bands (Kaufman *et al.* 1997b). The relationship between the middle-IR band and the visible bands varies as a function of time, vegetation type, and can vary within certain vegetation types by the internal structure of chlorophyll and water amount changes (Wen *et al.* 1999). Any deviation from the "mean relation" of the correlation then leads to a bias in the aerosol optical depth retrievals.

The over-land aerosol optical depth retrieval schemes are limited by high surface reflectance values, surface reflectance variability, and background type. High surface reflectance values will mask any radiance due to aerosols. Surface reflectance variability leads to biased aerosol optical depth retrievals due to departures from the "mean relation" between the middle-IR band and the visible bands. This also limits retrievals to multispectral satellite observations. The dark object approach is inherently limited to land areas that can support abundant vegetation. Many of the anthropogenic aerosols are generated in these regions, but mineral dust aerosols are largely produced in arid regions. Therefore, source regions for natural aerosols are largely neglected by the dark object approach.

D. AN ALTERNATIVE APPROACH TO OVER LAND AEROSOL OPTICAL DEPTH RETRIEVALS

Kaufman (1979) developed an analytical approximation for intensity of reflected radiation based on the radiative transfer equation and on the two-stream approximation from Coakley and Chylek (1975). The calculated intensity was used for the calculation of the atmospheric influence on the contrast between different adjacent surface reflectance values, or albedo, for two particular cases. Preliminary results indicated that this same method may be used to solve the radiative transfer equation for a non-uniform surface albedo and used to calculate the adjacency effects between areas of differing albedo.

The over-land aerosol optical depth retrieval approach proposed in this study uses the non-uniformity of different background types and evaluates contrast reduction due to various aerosols when viewed from near-zenith. Contrast reduction may be characterized by the standard deviation of the surface reflectance values or by the mean of adjacent pixel differences. The spectral distribution of the standard deviation and the mean across the visible spectrum in the absence of heavy aerosol loading can be used to characterize background types due to the wavelength dependence of surface albedo. Figure 1 shows that aerosols have unique spectral distributions of aerosol optical depth based on the size distribution of the particles. Likewise, the spectral distribution of contrast reduction can also be used to characterize the aerosol type due to its dependence on aerosol optical depth. Contrast reduction will be greater at wavelengths equivalent to or less than the aerosol particle size. Empirical relationships between contrast reduction and aerosol optical depth can be determined by comparison of calculated contrast reductions and ground or *in situ* aerosol optical depth measurements.

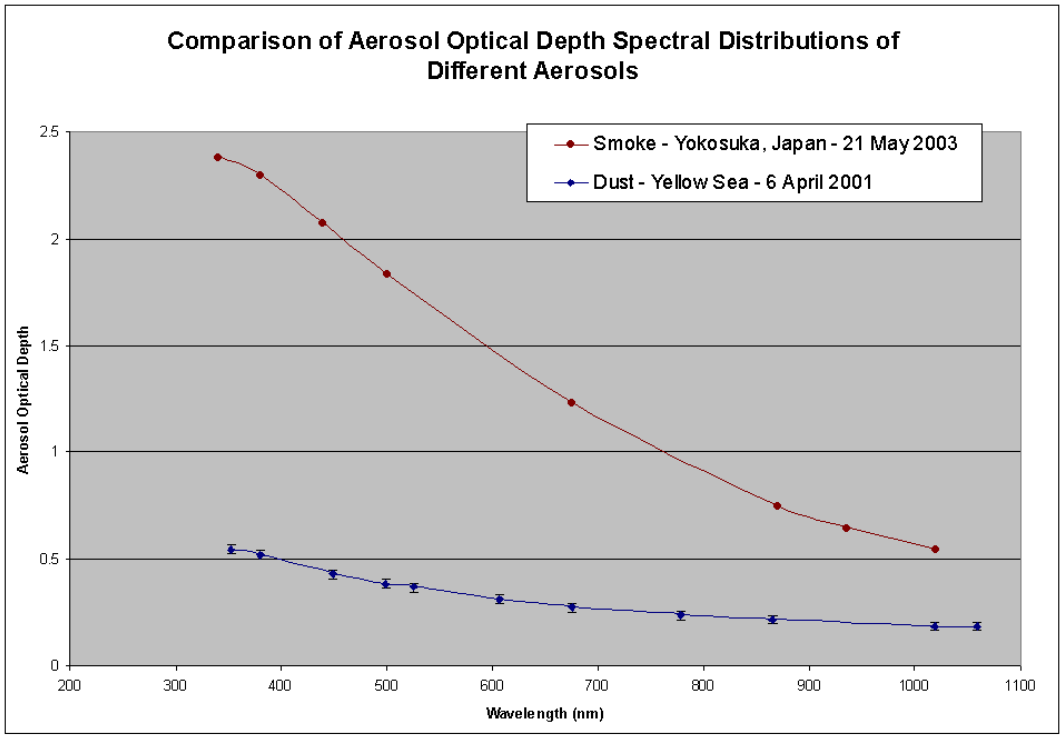

Figure 1. Comparison of Aerosol Optical Depth (AOD) Spectral Distributions of Different Aerosols.

THIS PAGE INTENTIONALLY LEFT BLANK

III. DATA

In order to validate the contrast reduction methods of aerosol optical depth and visibility proposed in this study, reference data sets were chosen based on the documented presence or absence of heavy aerosol loading. To the greatest extent possible, satellite observations of Japan were chosen within the same two-month window over a three-year period to reduce seasonal variability. This chapter will briefly describe the data sets and instrumentation used to collect the data in this study.

A. ACE-ASIA DATA SETS

The Aerosol Characterization Experiment-Asia (ACE-Asia) field experiment was the fourth in a series of Aerosol Characterization Experiments conducted by the International Global Atmospheric Chemistry Program (IGAC). As part of the experiment, an intensive field study was conducted between late March and May, 2001, in an effort to quantify the spatial and vertical distribution of aerosol concentrations and properties, the processes controlling their formation, evolution and fate, and the column integrated radiative effect of the aerosol (Huebert *et al.* 2003). During the intensive study period, a variety of aerosol conditions ranging from relatively clean to unusually heavy dust loading were observed and measured throughout East Asia using mobile and static platforms as well as satellite observations. The Earth Observing System (EOS) satellite, Terra, collected Moderate Resolution Imaging Spectroradiometer (MODIS) data during the period of intensive study as well.

B. INSTRUMENTS

1. Moderate Resolution Imaging Spectroradiometer (MODIS)

The MODIS instrument is a rotating scan mirror-type imager currently deployed aboard the Earth Observing System (EOS) satellites, Terra and Aqua, launched in 1999 and 2002, respectively. Both Terra and Aqua are polar-orbiting satellites with near-circular, sun-synchronous orbits with approximately 98.2 degrees of inclination at an

altitude of approximately 705 km (Goddard Space Flight Center, 2003). Terra, the "morning" satellite, was designed for a descending node equatorial crossing time of 10:30 a.m. local. Drag and inclination adjustments within the last year have caused delays in equatorial crossing time by as much as one hour, however (Brentzel 2003). Aqua, the "afternoon" satellite, has an ascending node equatorial crossing time of 1:30 p.m. local. MODIS measures radiant and solar-reflected energy from sampled areas of the Earth in 36 spectral bands between 0.415 and 14.385 μm. MODIS has nominal spatial resolutions of 250 m (2 bands), 500 m (5 bands), and 1000 m (29 bands) across a swath of 2330 km. Table 1 lists the primary use of each band and its maximum spatial resolution.

The MODIS data used in this study were acquired as part of the NASA's Earth Science Enterprise. The raw MODIS data were processed by the MODIS Adaptive Processing System (MODAPS) and Goddard Distributed Active Archive Center (DAAC), and are archived and distributed by the Goddard DAAC.

Primary Use	Band	Bandwidth[1]	Spatial Resolution[2]	Spectral Radiance[3]	Required SNR[4]
Land/Cloud/Aerosols Boundaries	1	620 - 670	250	21.8	128
	2	841 - 876	250	24.7	201
Land/Cloud/Aerosols Properties	3	459 - 479	500	35.3	243
	4	545 - 565	500	29.0	228
	5	1230 - 1250	500	5.4	74
	6	1628 - 1652	500	7.3	275
	7	2105 - 2155	500	1.0	110
Ocean Color/ Phytoplankton/ Biogeochemistry	8	405 - 420	1000	44.9	880
	9	438 - 448	1000	41.9	838
	10	483 - 493	1000	32.1	802
	11	526 - 536	1000	27.9	754
	12	546 - 556	1000	21.0	750
	13	662 - 672	1000	9.5	910
	14	673 - 683	1000	8.7	1087
	15	743 - 753	1000	10.2	586
	16	862 - 877	1000	6.2	516
Atmospheric Water Vapor	17	890 - 920	1000	10.0	167
	18	931 - 941	1000	3.6	57
	19	915 - 965	1000	15.0	250
Primary Use	**Band**	**Bandwidth[1]**	**Spatial Resolution[2]**	**Spectral Radiance[2]**	**Required NE[delta]T(K)[4]**
Surface/Cloud Temperature	20	3.660 - 3.840	1000	0.45(300K)	0.05
	21	3.929 - 3.989	1000	2.38(335K)	2.00
	22	3.929 - 3.989	1000	0.67(300K)	0.07
	23	4.020 - 4.080	1000	0.79(300K)	0.07
Atmospheric Temperature	24	4.433 - 4.498	1000	0.17(250K)	0.25
	25	4.482 - 4.549	1000	0.59(275K)	0.25
Cirrus Clouds Water Vapor	26	1.360 - 1.390	1000	6.00	150(SNR)
	27	6.535 - 6.895	1000	1.16(240K)	0.25
	28	7.175 - 7.475	1000	2.18(250K)	0.25
Cloud Properties	29	8.400 - 8.700	1000	9.58(300K)	0.05
Ozone	30	9.580 - 9.880	1000	3.69(250K)	0.25
Surface/Cloud Temperature	31	10.780 - 11.280	1000	9.55(300K)	0.05
	32	11.770 - 12.270	1000	8.94(300K)	0.05
Cloud Top Altitude	33	13.185 - 13.485	1000	4.52(260K)	0.25
	34	13.485 - 13.785	1000	3.76(250K)	0.25
	35	13.785 - 14.085	1000	3.11(240K)	0.25
	36	14.085 - 14.385	1000	2.08(220K)	0.35

[1] Bands 1 to 19 are in nm; Bands 20 to 36 are in μm
[2] Resolution at nadir in meters
[3] Spectral Radiance values are (W/m^2 -μm-sr)
[4] SNR = Signal-to-noise ratio
[5] NE(delta)T = Noise-equivalent temperature difference

Table 1 MODIS Channel Primary Use and Specifications (Adapted from GSFC 2003).

2. MODIS Data

The quality control and processing of the MODIS data are described by a series of levels ranging from 0 to 4 with successively higher processing corresponding to higher numbers (NASA 2003). Level 0 processing eliminates transmission errors, artifacts, and duplicate packets. The processed Level 0 data are then sent to the Distributed Active Archive Center (DAAC) for further processing. At the DAAC, the Level 0 data are processed to Level 1 data by combining ephemeris data with calibration information to produce geo-located radiance values and then partitioned into 5-minute granules representing approximately 2000 kilometers along the flight path. At this point, the bands for 250 meter, 500 meter, and 1000 meter data are separated into three files. For 1000 m and 500 m data, those bands with higher resolution (i.e. bands 1 through 7) are aggregated to the lower resolution.

ACE-Asia thoroughly documented the occurrence of heavy mineral dust loading during the spring 2001 intensive observation period. An independent field collection effort sponsored by the Naval Postgraduate School documented the presence of smoke from Siberian biomass burning over Japan during the period of 19 through 24 May 2003. MODIS data over Japan for 10 and 27 April 2001, and 21 May 2003 clearly delineating heavy mineral dust loading, absence of heavy aerosol loading, and heavy smoke loading respectively. Level 1B data were ordered from the GSFC DAAC for these dates at 1-kilometer resolution (Channels 1-36), 500-meter resolution (Channels 1-7), and 250-meter resolution (Channels 1 and 2). One-kilometer data included reflectance and reflected radiance data (Channels 1-19 and 26) and emissive radiance (Channels 20-36 excluding channel 26). Higher resolution data included only reflectance and reflected radiance data. Figure 2 shows 1-kilometer Level 1B true color composite images (Channels 1, 4, and 3) for (a) the low aerosol loading case (27 April 2001), (b) .the dust case (10 April 2001), and (c) the smoke case (21 May 2003).

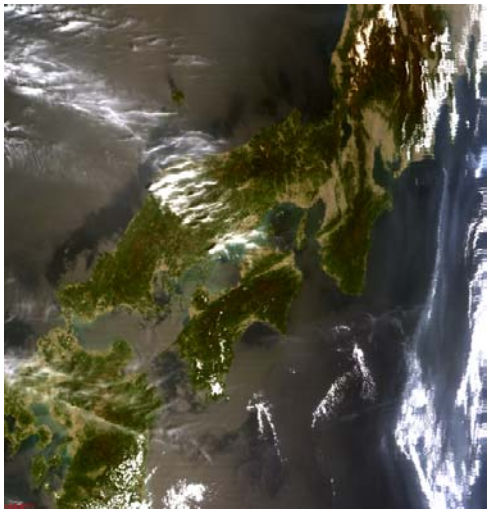
(a)

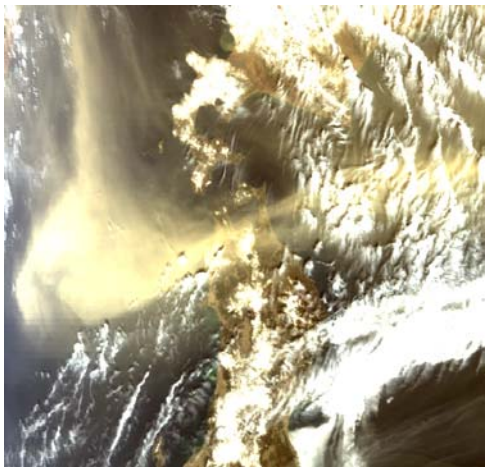
(b)

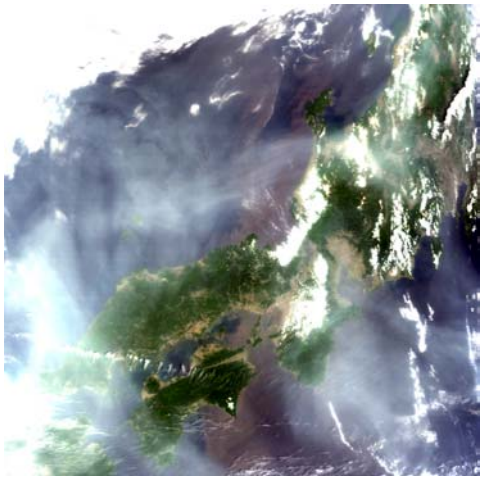
(c)

Figure 2. MODIS Level 1B 1-kilometer true color image (Channels 1, 4 and 3) of Japan under (a) low aerosol conditions at 0200 GMT 27 April 2001, (b) dust at 0135 GMT 10 April 2001, and (c) smoke at 0155 GMT 21 May 2003.

3. Microtops II hand-held Sun Photometer

The Microtops II hand-held sun photometer (hence forth the Microtops sun photometer) is a narrow field of view radiometer (Volz type) manufactured by Solar Light Incorporated (Morys *et al.* 1996). The Microtops sun photometer is widely used due to its ease of use, portability, and relatively low cost. The instrument uses photodiode detectors coupled with amplifiers and analog-to-digital converters and the collimators are mounted in a cast aluminum block with a full field of view of 2.5°. Data can be collected a five wavelengths that may be chosen by the interference filter installed. Two filter configurations were used in the NPS field collection effort. The first was the "ozone" configuration with wavelengths of 340, 380, 440, 500, and 675 nanometers. The second was the "water vapor" configuration with wavelengths of 500, 675, 870, 936, and 1020 nanometers. The instrument can collect aerosol optical depths, column ozone concentrations, and column water vapor concentrations based on the filter combination installed. These parameters are calculated in real-time by a built-in microprocessor and may be viewed on the LCD screen. The Microtops sun photometer may be ordered with built-in pressure and temperature sensors or such data may be entered manually. A Global Positioning System (GPS) connection allows for the collection of precise position and time. Data is collected by pointing the instrument at the sun and aligning the sun in a cross-hair screen. The user may adjust the sampling time and number of values used for averaging to achieve the reported result. Results are stored internally and may be recalled to the LCD screen or downloaded to a personal computer.

4. Microtops Data

An independent field collection effort sponsored by the Naval Postgraduate School documented the presence of smoke from Siberian biomass burning over Japan during the period of 19 through 24 May 2003. Microtops data were collected approximately every two to five minutes for a five-hour period on 21 May 2003 at Naval Station, Yokosuka, Japan. Porter et al. (2001) noted that if the Microtops sun photometer is not turned off between readings, the data may experience a bias when changes in the ambient temperature on the order of 30°C to 40°C are present during the collection

period. The instruments were not turned off between readings during this collection effort due to the time required for the initial diagnostics to run. The ambient temperature change during the collection effort was less than 2°C so any bias due to temperature change is assumed to be negligible. The data collected were used to construct the spectral signature of the smoke aerosol shown in Figure 1.

THIS PAGE INTENTIONALLY LEFT BLANK

IV. METHODS AND PROCEDURES

This chapter outlines the methods and procedures used to evaluate the contrast reduction due to heavy aerosol loading in visual satellite imagery. Small spectral and spatial subsets of MODIS data were sorted by aerosol type (low aerosol loading, heavy smoke, and heavy dust) and background type (urban, forested, and agricultural). Nine combinations of aerosol type and background type were evaluated (low aerosol loading - urban, low aerosol loading -forested, low aerosol loading -agricultural, smoke-urban, smoke-forested, smoke-agricultural, dust-urban, dust-forested, dust-agricultural).

A. SATELLITE IMAGE RETRIEVAL AND DISPLAY

Satellite image retrieval and display was performed using the Environment for Visualizing Images (ENVI) version 3.6 software and Interactive Data Language (IDL) version 5.6 by Research Systems, Incorporated. The ENVI software allows the display and enhancement of the Earth Observing System's MODIS data along with various other types of satellite data. Tools within ENVI include the ability to subset data spatially and spectrally, build and apply masks, and calculate statistics on the entire data set or subsets. IDL was used to script functions not inherent in ENVI.

B. CONTRAST REDUCTION FROM VARIATION OF REFLECTANCE (STANDARD DEVIATION METHOD)

For this investigation, contrast reduction was divided into three aerosol regimes and three background regimes. A true color image constructed in ENVI was used to ensure the presence or absence of aerosol prior to selecting a site for analysis. The cases selected were chosen for the presence of mineral dust from Asian continental source regions, smoke from the biomass burning in Siberia, and an absence of heavy aerosol loading. The United States Geological Survey (USGS) Land Use/Land Cover System from the Eurasia land cover characteristics database was used for the background surface determination (Anderson et al. 1976). The USGS Land Use/Land Cover System divides

land use into 24 categories. Several categories have been combined for the purpose of this investigation to define generic forested regions, agricultural sectors and grasslands, and urban areas. Figure 3 shows an example of land use over central Japan.

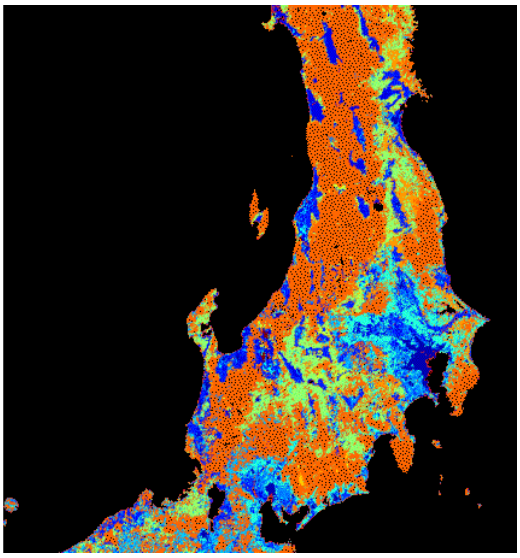

Figure 3. Example of U. S. Geological Survey Land Use/Land Cover System over central Japan (courtesy of Land Processes Distributed Active Archive Center).

Four to six areas were selected for each aerosol-background combination. Areas were defined by visual inspection using the Region of Interest (ROI) function in ENVI. The ROI function allows areas to be defined by a user created polygon. Uniform background types were identified using a visual inspection of the true color image in conjunction with the USGS Land Use/Land Cover System image of Japan. Figure 4 shows the regions of interest for (a) the forested background, (b) the urban background, and (c) the agricultural background for the smoke case on 21 May 2003. Channel 20 (3.660 to 3.840 micrometers), a thermal band, was used to delineate background-type boundaries where the true color image showed little distinction between background types. The variation in emissivity, or the ratio of flux emitted by an object to that emitted by a blackbody at the same temperature, for each background type provided strong thermal contrasts between background regions where little contrast in the visible wavelengths existed (Boyd 1988).

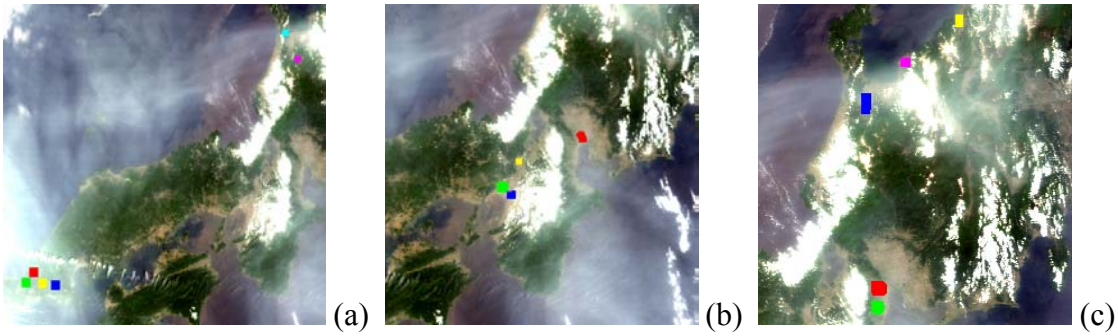

Figure 4. Regions of Interest (ROI) for (a) the forested background type, (b) the urban background type, and (c) the agricultural background type based on the MODIS image for the smoke case on 21 May 2003.

The standard deviation of the reflectance values was calculated for all visual channels in each region. The standard deviation for channels 12 through 16 failed to register for many cases due to saturation of the bands. These bands were originally optimized for ocean color applications. As such, the maximum spectral radiance allowed by the sensor was exceeded over land. The resulting standard deviations were then plotted as a function of wavelength by aerosol and background type. Several cases showed exceptionally high standard deviations in channels 10 and 11. Upon inspection, cloud contamination was found to be the main culprit. The reflectance due to cloud was identified by plotting a histogram of the reflectance values in the contaminated region. Cloud contamination was then filtered using a band pass mask excluding the cloud reflectance. The standard deviations were again calculated for those channels using the band pass mask and found to be more in line with expected values. The average standard deviation was determined for each channel in the background/aerosol groupings and the standard deviation of the values in each channel was used to define the relative variability.

The effects of resolution were also investigated. In the MODIS sensor, the first two channels have an optimum resolution of 250 meters and channels three through seven have an optimum resolution of 500 meters. Because these channels are aggregated to form lower resolution images at the 1-kilometer resolution, they provide an excellent data set to gauge variability due to changes in resolution. The low aerosol loading-urban case was chosen for this test due to its high variability at smaller spatial scales. The process described in the previous paragraphs was applied to channels one through seven

for the 500-meter resolution data and to channels one and two for the 250-meter data for the same low aerosol loading-urban cases used earlier.

C. CONTRAST REDUCTION FROM VARIATION OF REFLECTANCE (DIFFERENCING METHOD)

An alternative method of evaluating contrast reduction using differences between adjacent pixels was also explored. Differences between adjacent pixels to the right and below were calculated separately and then summed to enhance contrast boundaries. The mean of this summed difference field was then determined for each channel.

For this part of the investigation, the same cases were used for each of the nine combinations of aerosol and background type as used previously. The region subsets were exported to an IDL variable using the ENVI export function prior to any statistical calculation. The export function, however, includes all pixels in a rectangle based on the most extreme points of the ROI's polygon and therefore included more data than the regions used in the first part of the investigation. An IDL program was then used to:

- Read in the variable,
- Divide the region subset into 22 separate channel variables,
- Difference each channel to the right and down,
- Sum the difference fields, and
- Determine the mean of each summed difference field.

Many of the problems experienced in the standard deviation analysis were encountered again for the difference analysis. Channels 12 through 16 showed signs of total saturation in fewer cases than seen using the standard deviation method described previously. Visual inspection of cases where channels 12 through 16 did not experience total saturation showed at least partial saturation over land, making the results suspect at best.

Again, several cases showed exceptionally high standard deviations in channels 10 and 11. These outliers were attributed to contamination due to clouds or water that was unintentionally included in the export process. This contamination proved difficult to remove by a filtering process. Unsuccessful attempts were made to apply a cloud and

water masks prior to exporting the data. Also unsuccessful were attempts to apply the previously generated mask to the summed difference fields. These failures were attributed to the fact that IDL assigns a value of zero to masked pixels instead of a missing data or "Not a Number (NaN)" value. The masked pixels continued to be used in the statistical calculations and created large differences along the mask boundaries comparable to that created by the cloud or water boundaries. The values within the mask were shifted in the same manner as the data channels and summed with the original mask to create a more conservative mask. This conservative mask was applied to the final summed difference field prior to the mean calculation, thus removing the exceptionally high differences. The final result more closely matched those cases not contaminated by clouds or water.

THIS PAGE INTENTIONALLY LEFT BLANK

V. RESULTS

A. AEROSOL REGIME ANALYSIS – 27 APRIL 2001

The Terra MODIS observations over Japan for the date of 27 April 2001 represent atmospheric conditions with minimal influence from continental natural or anthropogenic aerosols. Maritime aerosols dominate the aerosol size and concentration distributions over Japan at this time. Anthropogenic aerosols are likely present in the vicinity of urban areas, but the maritime aerosol regime appears to dominate from visual inspection of the imagery. Four to six cases for each background type (forested, urban, and agricultural) have been chosen for analysis. All cases were chosen as close to the sensor zenith as possible to prevent reductions in observed contrast due to low view angles.

1. Standard Deviation Method

Four to six cases throughout central and southern Japan were chosen for each background type. Polygons were constructed to define the selected areas limited to a common background type and excluded any cloud contamination. Each area covered approximately 200 square kilometers. Standard deviations for the surface reflectance values were calculated for the visible MODIS channels (channels 1 through 19 and 26) in each of the polygons. The average standard deviations of surface reflectance for the cases in each background type were calculated for each channel. The standard deviation of the standard deviation values in the cases in each channel was used as a measure of variability of a low aerosol regime over a given background type.

Standard deviation calculations failed for over 50% of the cases for channels 13 through 16, centered at 667, 678, 748 and 870 nanometers respectively. Channels 13 and 14 include both high and low gain measurements.

Saturation of channels 13 through 16 results from the designed radiometric response set before launch. High gain measurements consistently saturate over land. Low gain measurements saturated over 50% of the time over land. MODIS channels 8 through 16 are optimized for ocean color applications and the maximum measurable

spectral radiance is relatively low in channels 13 through 16. Over land, these channels tend to saturate frequently. Channels 13 through 16 have been excluded from the calculations for the standard deviation method leaving a gap between 700 and 800 nanometers in the spectral distribution of standard deviations. Figure 5 shows a comparison of the spectral plots of average standard deviation of surface reflectance for each background type on 27 April 2001.

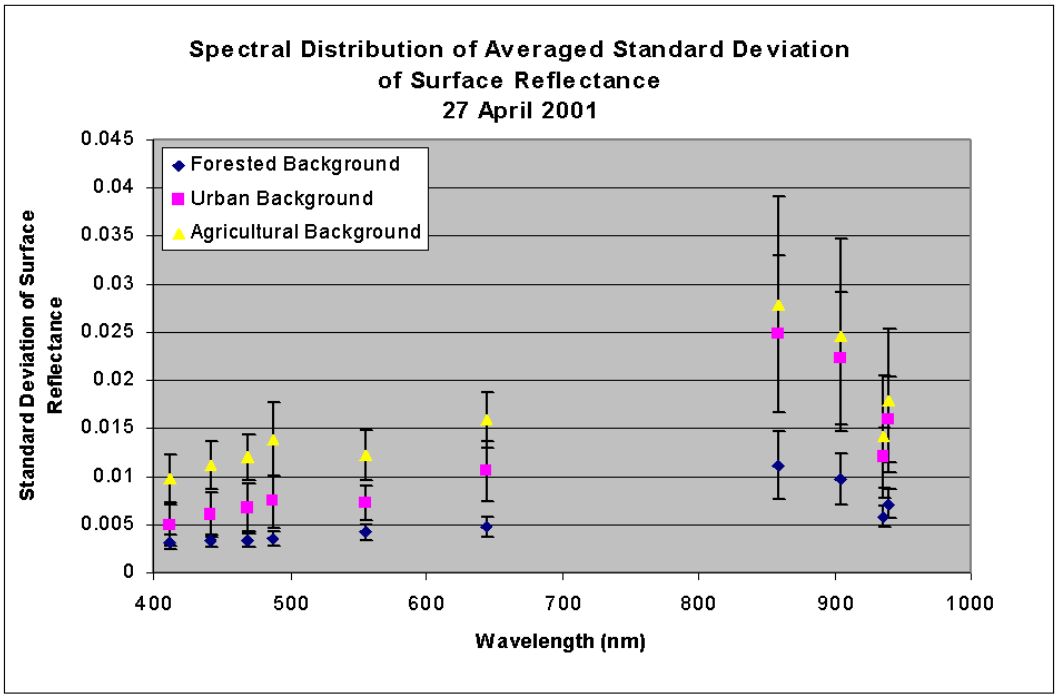

Figure 5. Spectral Distribution of Averaged Standard Deviation of Surface Reflectance as measured by MODIS for 27 April 2001 (Low Aerosol Loading Case).

a. Forested Background

Six cases were selected covering the forested mountain regions of central and southern Japan. In Figure 5, the absolute average standard deviation for the forested background in the visible end of the spectrum, 400 through 700 nanometers, was found to be less than 0.005, the lowest of all background types studied. The absolute average standard deviation in the near-infrared region of the spectrum, 800 through 1000 nanometers, was found to be approximately 0.01, also the lowest of all background types studied. Variability within each channel as measured by the standard deviation of the six

cases was the lowest for all background types studied. This exceptionally low variability reduces the effectiveness of the variability techniques as the addition of aerosol lowers the already low variability. The "dark object" approach, however, is proven and effective of large forested areas and is likely more appropriate for the forested background type.

The shape of the average spectral distribution of standard deviation in Figure 5 for the forested region shows a linear increase in the visible region. The average spectral distribution of standard deviation in the near-infrared region shows a decreasing trend between 860 and 936 nanometers with a negative slope ten times greater than in the visible region followed by a sharp increase to 940 nanometers. The sharp contrast between 936 and 940 nanometers, Channels 18 and 19 respectively, are seen consistently with all background and aerosol types and is attributed to their proximity to the wings of water vapor absorption band.

b. Urban Background

Five cases were selected covering major urban centers in southern and central Japan. In Figure 5, the absolute average standard deviation for the urban background type in the visible end of the spectrum ranged from 0.005 to 0.01. The urban background showed a distinctive spectral shape in the visible region. The average standard deviation showed peaks of approximately 0.0075 and 0.01 at 488 and 645 nanometers respectively. The absolute average standard deviation in the near-infrared region of the spectrum ranged from over 0.01 to 0.025 and exhibited the same spectral shape seen in the forested case due to the proximity to the water vapor absorption band. The variability of the standard deviations was two to three times that seen in the forested case in both the visible and near-infrared regions.

c. Agricultural Background

Five cases were selected covering agricultural areas in southern and central Japan. In Figure 5, the absolute average standard deviation of the agricultural background in the visible end of the spectrum ranged from approximately 0.01 to just over 0.015. The agricultural background showed a spectral shape in the visible region

similar to that of the urban background in Figure 5. The average standard deviation and the variability of the agricultural background were the highest for all background types in Figure 5. The average standard deviation showed peaks of over 0.013 and just over 0.015 at 488 and 645 nanometers respectively. The absolute average standard deviation in the near-infrared region of the spectrum for the agricultural background ranged from below 0.015 to just below 0.03 and exhibited the same spectral shape seen in the forested case in Figure 5 due to the proximity to the water vapor absorption band. The variability of the standard deviations in the visible region was similar to that seen in the urban background in Figure 5. The variability in the near-infrared region was approximately double that seen in the urban background. The similar spectral shape is attributed to the similar scales of variability between the urban and agricultural backgrounds. The agricultural practices of Japan result in a crop size scales similar to that of buildings in an urban area. Such agricultural size scales are likely unique to Japan and similar cultures and may not be applicable to large areas of open agriculture such as seen in the central United States.

Figure 5 shows that in the absence of heavy aerosol loading different background types have unique spectral signatures. The standard deviation of the standard deviations is used as a measure of variability. Here, the background types exhibit little overlap in spectral signatures in the visible region. This result may be used to discriminate background types based on spectral signature.

2. Differencing Method

The differencing method of variability assessment was applied to the same cases for each background type used in the standard deviation method. The areas used for the differencing were rectangles containing the polygons defined for the standard deviation method. Each area covered approximately 300 square kilometers and was not necessarily free of cloud or surface water contamination. The differences in surface reflectance values between each pixel and the adjacent pixel to the right and below were taken separately. The resulting difference fields were summed for each of the visible MODIS channels (channels 1 through 19 and 26) in each of the cases. The mean was calculated for each of the summed difference fields. The average mean of differenced surface reflectance for the cases in each background type were calculated for each channel. The

standard deviation of the mean values in the cases in each channel was used as a measure of variability of a low aerosol regime over a given background type. Mean calculations failed for over 50% of the cases for Channels 13 through 16. These channels have been excluded from the calculations for the differencing method leaving a gap between 700 and 800 nanometers in the spectral distribution of mean differences in surface reflectance. Figure 5 shows a comparison of the spectral plots of averaged mean differenced surface reflectance for each background type on 27 April 2001.

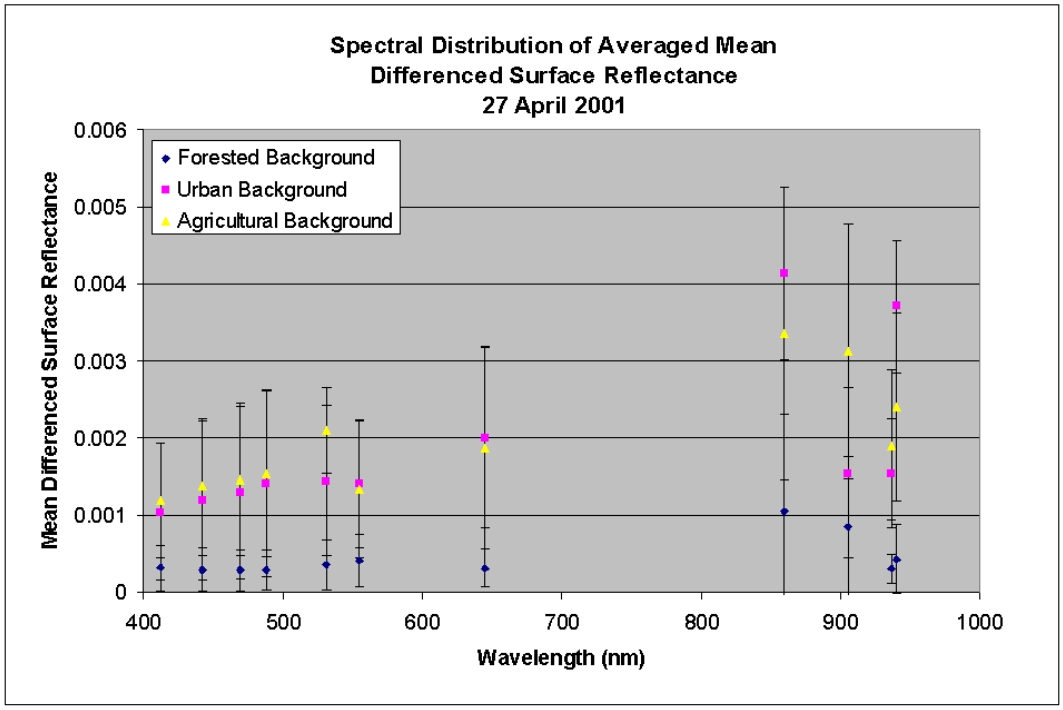

Figure 6. Spectral Distribution of Averaged Mean Differenced Surface Reflectance as measured by MODIS for 27 April 2001 (Low Aerosol Loading Case).

a. Forested Background

The same six cases covering the forested mountain regions of central and southern Japan were used for the differencing method. In Figure 6, the absolute average mean differenced surface reflectance in the visible end of the spectrum increased linearly and was the lowest of all background types studied. The absolute average mean differenced surface reflectance in the near-infrared region of the spectrum for the forested

background was also the lowest of all background types studied. Variability within each channel as measured by the standard deviation of the six cases was the lowest for all background types studied. The near-infrared region for the forested background type shown in Figure 6 exhibited the same spectral shape seen in the standard deviation method attributed to the proximity of the channels to the water vapor absorption band.

b. Urban Background

The same five cases covering major urban centers in central and southern Japan were used in the differencing method. The urban background in Figure 6 again showed a distinctive spectral shape in the visible region as it did in Figure 5. The average mean differenced surface reflectance for the urban background in the visible region peaked at approximately 0.0015 and 0.002 at 488 and 645 nanometers respectively. The average mean differenced surface reflectance in the near-infrared region of the spectrum ranged from approximately 0.015 to 0.04. The urban background type for low aerosol loading is the only case where the near-infrared signature did not exhibit the same spectral shape seen in the forested case due to the proximity to the water vapor absorption band. The only deviation is a significant dip at 905 nanometers of the same order as that seen at 936 nanometers as seen in Figure 6. The variability of the standard deviations was twice that seen in the forested case in both the visible and near-infrared regions.

c. Agricultural Background

The same five cases were covering agricultural areas in central and southern Japan were used in the differencing method. In Figure 6, the average mean differenced surface reflectance for the agricultural background in the visible end of the spectrum peaked at approximately 0.002 at 531 and 645 nanometers respectively. The agricultural background showed a spectral shape in the visible region similar to that of the urban background in Figure 6 with the exception of the significant peak at 531 nanometers. The average mean differenced surface reflectance was higher than or comparable to that of the urban background type in Figure 6 with variability similar to

that of the urban background. The average mean differenced surface reflectance in the near-infrared region of the spectrum for the agricultural background type ranged from 0.002 to just over 0.003 and exhibited the same spectral shape seen in the forested case due to the proximity to the water vapor absorption band. The variability of the mean differences in the visible region of the agricultural background as measured by the standard deviations was similar to that seen in the urban background in Figure 6. The variability in the near-infrared region was of the same order of that seen in the urban background in Figure 6. A discussion of the similarities between the agricultural and urban backgrounds can be found in the standard deviation method section.

B. AEROSOL REGIME ANALYSIS – 10 APRIL 2001

The Terra MODIS observations over Japan for the date of 10 April 2001 represent atmospheric conditions dominated by mineral dust from the Asian continent. Anthropogenic aerosols are likely present in the vicinity of urban areas, but the dust regime dominates in the urban area chosen from visual inspection of the imagery. Four to five cases for the agricultural and forested background types have been chosen for analysis. Only one urban case could be clearly identified from imagery due to the nature of the dust plume from the Asian continent. All cases were chosen as close to the sensor zenith as possible to prevent reductions in observed contrast due to low view angles.

1. Standard Deviation Method

Four to five cases for the agricultural and forested background type and one case for the urban background type were chosen throughout northern Japan. Polygons were constructed to define the selected areas limited to a common background type and excluded any cloud contamination. Each area covered approximately 200 square kilometers. Standard deviations for the surface reflectance values were calculated for the visible MODIS channels (channels 1 through 19 and 26) in each of the polygons. The average standard deviations of surface reflectance for the cases in each background type were calculated for each channel. The standard deviation of the standard deviation values

in the cases in each channel was used as a measure of variability of a dust regime over a given background type. Standard deviation calculations failed for over 50% of the cases for Channels 11 through 16, centered at 531, 555, 667, 678, 748 and 870 nanometers respectively. Both Channels 13 and 14 high and low gain measurements consistently saturated over land. See the previous section for a discussion of limitations of Channels 8 through 16. Channels 11 through 16 have been excluded from the calculations for the standard deviation method. Figure 7 shows a comparison of the spectral plots of average standard deviation of surface reflectance for each background type on 10 April 2001.

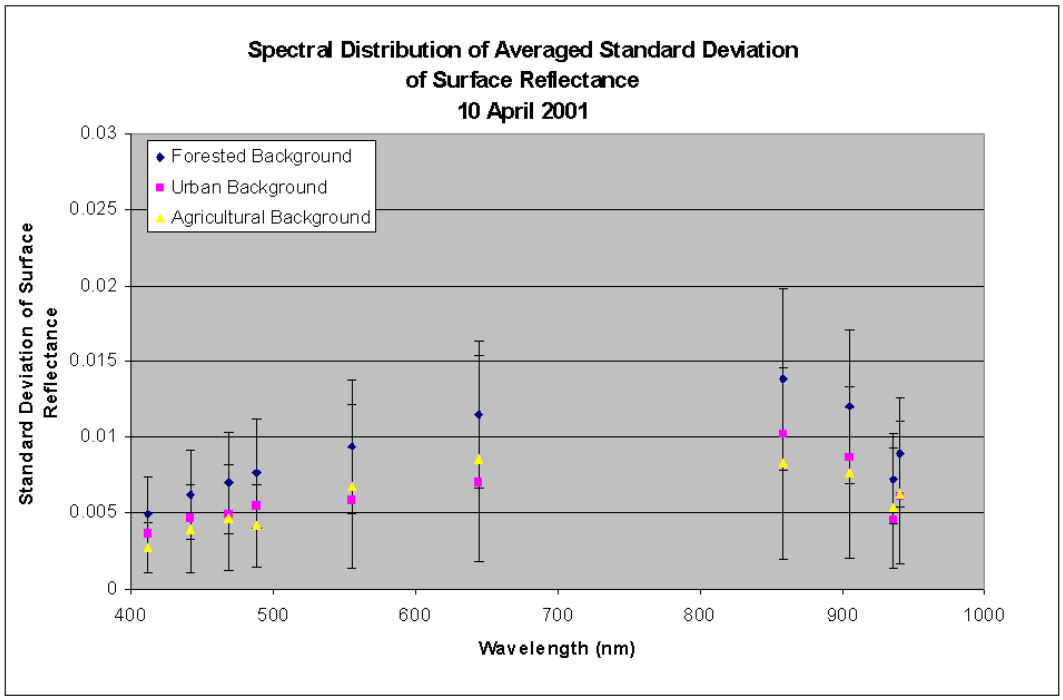

Figure 7. Spectral Distribution of Averaged Standard Deviation of Surface Reflectance as measured by MODIS for 10 April 2001 (Dust Case).

a. Forested Background

Five cases were selected covering the forested mountain regions of northern Japan. In Figure 7, the absolute average standard deviation in the visible end of the spectrum was found to be less than 0.012. The absolute average standard deviation in the near-infrared region of the spectrum for the forested background ranged was less than

0.014. Variability within each channel as measured by the standard deviation of the five cases was the two to five times of that seen in the low aerosol regime in Figure 5.

The shape of the average spectral distribution of standard deviation for the forested region in Figure 7 shows a linear increase in visible spectrum similar to that seen in the low aerosol regime in Figure 5 but with a slope four times larger. The average spectral distribution of standard deviation in the near-infrared region shows a decreasing trend between 860 and 936 nanometers followed by a less pronounced increase to 940 nanometers. The slope of the line between 859 and 905 nanometers in Figure 7 is twice the value of that seen in the low aerosol case in Figure 5.

The dust-forested background case in Figure 7 was the only case to exhibit an increase in contrast in the presence of heavy aerosol loading. Visual inspection of the MODIS image revealed striations in the plume of dust in the study area. It is thought that the nature of the dust plume added contrast and variability to what is normally a low contrast background with low variability. The limitations of the contrast method with respect to the forested case are discussed above.

b. Urban Background

Only one case of a dust regime dominating a major urban center in northern Japan was identified. In Figure 7, the absolute average standard deviation in the visible end of the spectrum was less than 0.007. The dust regime as characterized in Figure 7 showed the expected decrease in standard deviation. The urban background in the presence of dust also showed the same distinctive spectral shape in the visible region as seen in Figure 5. Figure 7 shows average standard deviation increased linearly with peaks of just over 0.005 at 488 and 555 nanometers and a peak of 0.007 at 645 nanometers. The absolute average standard deviation in the near-infrared region of the spectrum for the urban background was less than 0.01, half of that seen in the low aerosol loading case, and exhibited the water vapor absorption band spectral. The variability of the standard deviations could not be determined due to the limited number of urban cases.

c. Agricultural Background

Four cases were selected covering agricultural areas in northern Japan. In Figure 7, the absolute average standard deviation in the visible end of the spectrum was below 0.009. The agricultural background under the influence of the dust regime shown in Figure 6 showed the same spectral shape across the entire spectrum as seen in the low aerosol case in Figure 5 but with lower average standard deviations and variability in all channels. The average standard deviation of the agricultural background showed two peaks of approximately 0.005 and 0.009 at 469 and 645 nanometers respectively. The absolute average standard deviation in the near-infrared region of the spectrum for the agricultural background ranged from approximately 0.005 to 0.008, roughly one-third of that seen for the agricultural case in the low aerosol loading case in Figure 5, and exhibited the typical water vapor absorption band spectra. The contrast reduction was greatest in the near-infrared region.

2. Differencing Method

The differencing method of variability assessment was applied to the same cases for each background type used in the standard deviation method. The areas used for the differencing were rectangles containing the polygons used for the standard deviation method. Each area covered approximately 300 square kilometers and was not necessarily free of cloud or water contamination. The differences in surface reflectance values between each pixel and the adjacent pixel to the right and below were taken separately. The resulting difference fields were summed for each of the visible MODIS channels (channels 1 through 19 and 26) in each of the cases. The mean was calculated for each of the summed difference fields. The average mean of differenced surface reflectance for the cases in each background type were calculated for each channel. The standard deviation of the mean values in the cases in each channel was used as a measure of variability of a dust regime over a given background type. Mean calculations failed for over 50% of the cases for Channel 11 and for all cases for Channels 12 through 16. Channels 11 through 16 have been excluded from the calculations for the differencing

method. Figure 8 shows a comparison of the spectral plots of average mean differenced surface reflectance for each background type on 10 April 2001.

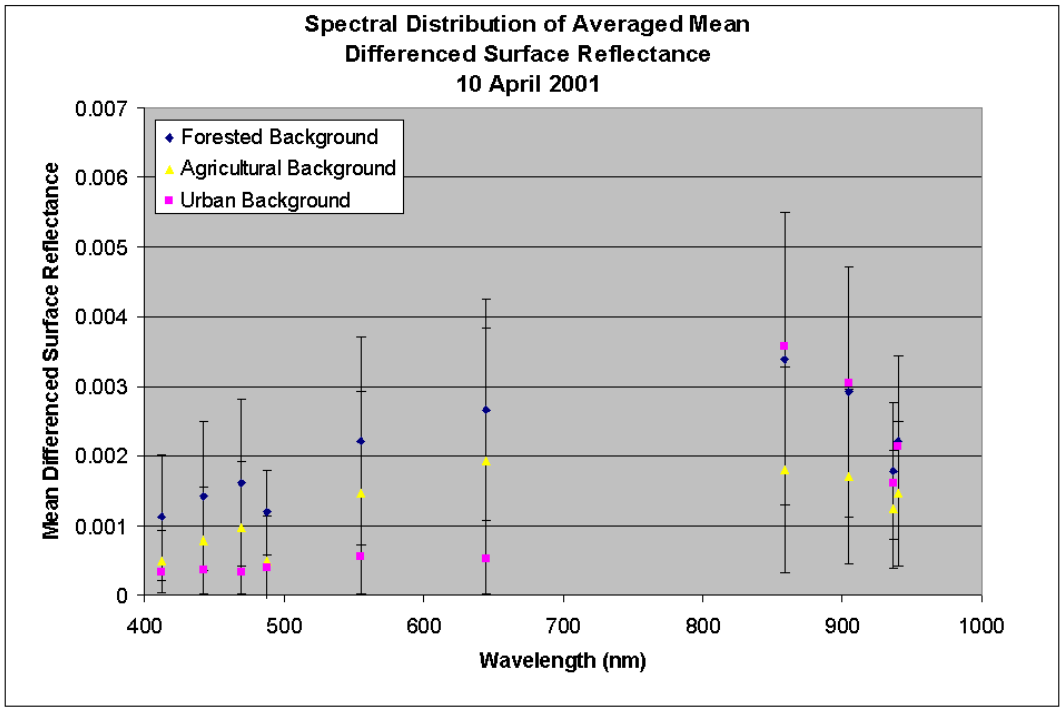

Figure 8. Spectral Distribution of Averaged Mean Differenced Surface Reflectance as measured by MODIS for 10 April 2001 (Dust Case).

a. Forested Background

The same five cases covering the forested mountain regions of northern Japan were used for the differencing method. In Figure 8, the absolute average mean differenced surface reflectance in the visible end of the spectrum for the forested background increased linearly to 0.0025, with the exception of a value of just over 0.01 at 488 nanometers (channel 10). Channel 10 was contaminated with high surface reflectance values due to a body of water in the image subset. Two areas were excluded due to exceptionally high values of mean differenced surface reflectance. This removal of outliers likely caused an over-correction resulting in a low bias in the channel 10 average for the forested background in Figure 8. It is thought that a conservative water mask would reduce both the absolute average mean differenced surface reflectance and the variability of the differenced surface reflectance values. The absolute average mean

differenced surface reflectance in the near-infrared region of the spectrum for the forested background ranged from approximately 0.0015 to 0.0035. Variability within each channel as measured by the standard deviation of the five cases used to determine the mean for the forested background in Figure 8 was two to five times that of the low aerosol loading case over the forested background in Figure 6. The near-infrared region for the forested background in Figure 8 exhibited the same spectral shape seen in the standard deviation method in Figure 7, but with more pronounced differences between the maximum and minimum values. Variations in magnitude of the spectral shape in the near-infrared region are likely due to variations in vegetation type. Radiometric response in the near-infrared region is highly dependent on the vegetation type and moisture content of the soil. Cases showing high variations are likely those with a wide range of vegetation types and varying soil moisture content.

b. Urban Background

The same case covering a major urban center in northern Japan were used in the differencing method. In Figure 8, the spectral shape of the urban background showed a linear trend in the visible region peaking at 0.0005. The results were inconclusive due to restriction to one case. The absolute mean differenced surface reflectance in the near-infrared region for the urban background exhibited a spectral shape that resembled a muted signature of the forested case in Figure 8. See discussion in previous section. The variability of the standard deviations was unavailable due to the limited number of cases.

c. Agricultural Background

The same four cases were covering agricultural areas in northern Japan were used in the differencing method. In Figure 8, the absolute average mean differenced surface reflectance in the visible end of the spectrum for the agricultural background showed the same linear spectral shape see in the forested region but at half of the magnitude of that seen in the forested region in Figure 8. The variability was of the same magnitude seen in the forested case in Figure 8. As in the forested case, two cases

showed exceptionally high values of mean differenced surface reflectance and were excluded as outliers. Again, conservative water and cloud masks should remedy this problem and bring values in line with expectations. The absolute average standard deviation in the near-infrared region of the spectrum showed the typical spectral shape due to the water vapor absorption band at half the magnitude seen in the forested case in Figure 8.

C. AEROSOL REGIME ANALYSIS – 21 MAY 2003

The Terra MODIS observations over Japan for the date of 21 May 2003 represent atmospheric conditions dominated by anthropogenic smoke from biomass burning in Siberia. Four to five cases for all background types have been chosen for analysis based on the presence of smoke from visual inspection of imagery. All cases were chosen as close to the sensor zenith as possible to prevent reductions in observed contrast due to low view angles.

1. Standard Deviation Method

Four to five cases for each background type were chosen throughout central and southern Japan. Polygons were constructed to define the selected areas and were limited to a common background type and excluded any cloud contamination. Each area covered approximately 200 square kilometers. Standard deviations for the surface reflectance values were calculated for the visible MODIS channels (channels 1 through 19 and 26) in each of the polygons. The average standard deviations of surface reflectance for the cases in each background type were calculated for each channel. The standard deviation of the standard deviation values in the cases in each channel was used as a measure of variability of a smoke regime over a given background type. Standard deviation calculations failed for over 50% of the cases for channels 10 and 11, centered at 488 and 531 nanometers respectively. Channels 12 through 16 failed for all cases due to saturation of the channel over land. See the previous section for a discussion of limitations of Channels 8 through 16. Channels 10 through 16 for the forested background and channels 11 through 16 for urban and agricultural backgrounds have

been excluded from the calculations for the standard deviation method. Figure 9 shows a comparison of the spectral plots of average standard deviation of surface reflectance for each background type on 21 May 2003.

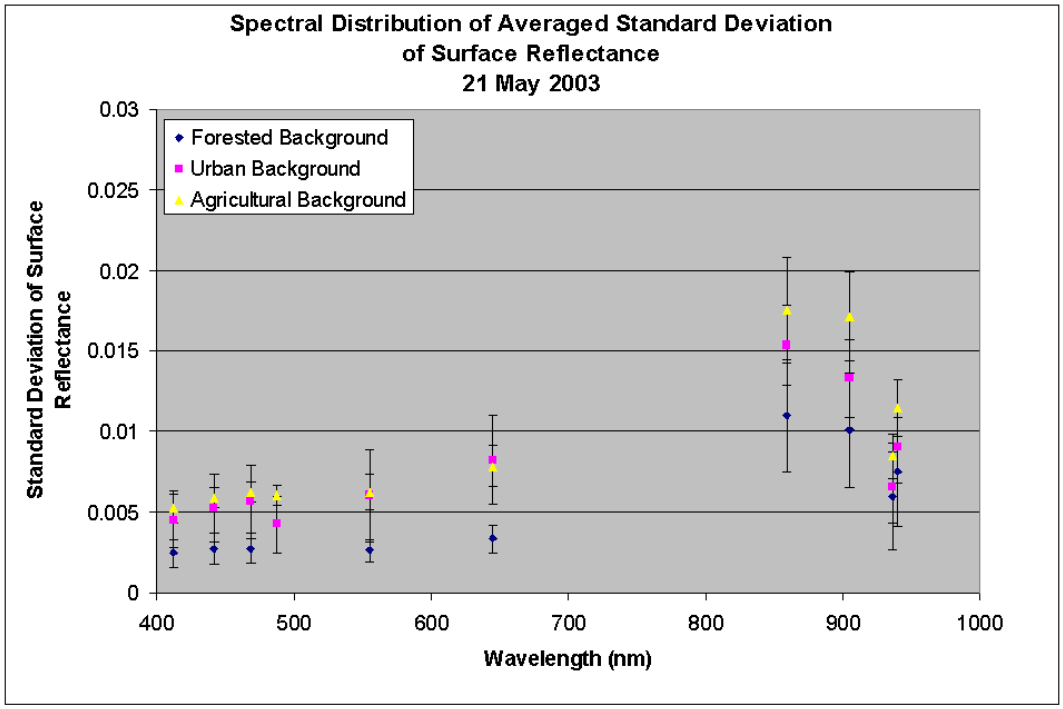

Figure 9. Spectral Distribution of Averaged Standard Deviation of Surface Reflectance as measured by MODIS for 21 May 2003 (Smoke Case).

a. Forested Background

Five cases were selected covering the forested mountain regions of central and southern Japan. In Figure 9, the absolute average standard deviation in the visible end of the spectrum peaked at approximately 0.0035. The absolute average standard deviation in the near-infrared region of the spectrum for the forested background ranged from 0.006 to 0.01. Variability within each channel as measured by the standard deviation of the five cases for the forested background was on the same order of that seen in the low aerosol regime in Figure 5.

The shape of the average spectral distribution of standard deviation for the forested region in Figure 9 shows a linear increase in visible spectrum between 412 and 469 nanometers. The standard deviation remains constant through 600 nanometers and

slightly increases at 645 nanometers. This is a significant deviation from linearly increasing spectral shape seen in the other two aerosol regimes for the forested background type seen in Figures 4 and 6. Takemura *et al.* (2002) generalized the single scatter albedo as a function of wavelength for carbonaceous aerosols for an aerosol modeling effort. The carbonaceous aerosol shows a peak in single scatter albedo at approximately 500 nanometers. This relatively high single scatter albedo at 500 nanometers is one explanation for the contrast reduction seen between 500 and 600 nanometers that is seen in the smoke aerosol regime in Figure 9 but not in the others. The average spectral distribution of standard deviation in the near-infrared region for the forested background shows the same shape and magnitude of standard deviation as seen in the low aerosol case in Figure 5.

b. Urban Background

Four cases covering major urban centers in central and southern Japan were selected. In Figure 9, the absolute average standard deviation in the visible end of the spectrum peaked at approximately 0.008. The absolute average standard deviation in the near-infrared region of the spectrum for the urban background showed the same spectral shape as seen in the low aerosol loading case in Figure 5, but with a lesser magnitude. The smoke regime depicted in Figure 9 showed the expected decrease in standard deviation due to contrast reduction. In Figure 9, variability in the visible region of the spectrum is of the same order of that seen in the low aerosol regime over an urban background in Figure 5. The variability in the near-infrared region was one-third of that seen with the low aerosol regime over the urban background in Figure 5.

In Figure 9, the shape of the average spectral distribution of standard deviation for the urban background shows a linear increase in the visible spectrum between 412 and 469 nanometers. The standard deviation dips to its lowest average value at 488 nanometers. A similar decrease in standard deviation, but smaller in magnitude, is seen at 488 nanometers for all background types in Figure 9. The combination of urban pollution and the carbonaceous smoke may account for the exceptionally high reduction in contrast at 488 nanometers over urban backgrounds. See the discussion of the wavelength dependence of single scatter albedo of carbonaceous

aerosols in the previous section. The average spectral distribution of standard deviation in the near-infrared region shows the same shape but a lesser magnitude of both standard deviation and variability as seen in the low aerosol case.

c. Agricultural Background

Five cases were selected covering agricultural areas in central and southern Japan. In Figure 9, the absolute average standard deviation in the visible end of the spectrum for the agricultural background peaked at 0.008. The agricultural background under the influence of the smoke regime showed the same spectral shape across the entire spectrum as seen in the low aerosol case as seen in Figure 5 but with lower average standard deviations and variability in all channels. The average standard deviation increased linearly between 412 to 469 nanometers decreased slightly at 488 nanometers and then increased at 555 and 645 nanometers. In Figure 9, the absolute average standard deviation in the near-infrared region of the spectrum exhibited the typical water vapor absorption band spectral shape with values of the same order as seen in the low aerosol loading case in Figure 5.

2. Differencing Method

The differencing method of variability assessment was applied to the same cases for each background type used in the standard deviation method. The areas used for the differencing were rectangles containing the polygons used for the standard deviation method. Each area covered approximately 300 square kilometers and was not necessarily free of cloud or water contamination. The differences in surface reflectance values between each pixel and the adjacent pixel to the right and below were taken separately. The resulting difference fields were summed for each of the visible MODIS channels (channels 1 through 19 and 26) in each of the cases. Means were calculated for each of the summed difference fields. The average means of differenced surface reflectance for the cases in each background type were calculated for each channel. The standard deviation of the mean values in the cases in each channel was used as a measure of variability of a smoke regime over a given background type. Mean calculations failed

for over 50% of the cases for channels 10 and 11 for the forested background type and for all cases for channels 12 through 16. Channels 11 through 16 have been excluded from the calculations for the differencing method. Figure 10 shows a comparison of the spectral plots of average standard deviation for differenced surface reflectance for each background type on 10 April 2001.

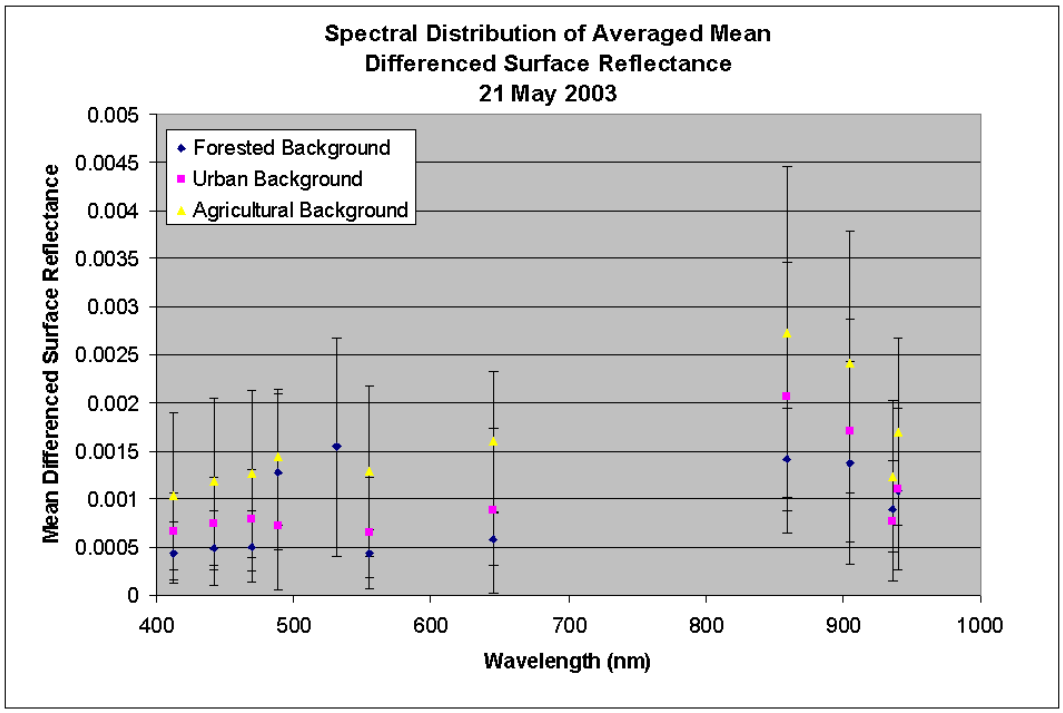

Figure 10. Spectral Distribution of Averaged Mean Differenced Surface Reflectance as measured by MODIS for 21 May 2003 (Smoke Case).

a. Forested Background

The same five cases covering the forested mountain regions of central and southern Japan were used for the differencing method. In Figure 10, the absolute average mean differenced surface reflectance in the visible end of the spectrum for the forested background shows a linear increase between 412 and 469 nanometers followed by a two-fold increase at 488 and 531 nanometers. The original linear trend is resumed at 555 nanometers and continues to 645 nanometers. In Figure 10, the absolute average mean differenced surface reflectance in the near-infrared region of the spectrum was the lowest of all background types in the smoke regime and showed the typical water vapor

absorption band signature. Variability within each channel as measured by the standard deviation of the five cases was two to five times of that of the low aerosol loading case over the forested background in the visible region as seen in Figure 6 and of the same order as that seen in the near-infrared region in the low aerosol regime in Figure 6.

b. Urban Background

The same four cases covering major urban centers in central and southern Japan were used in the differencing method. In Figure 10, the absolute average mean differenced surface reflectance in the visible end of the spectrum showed peaks of 0.0008 and 0.0009 and 469 and 645 respectively. The absolute average mean differenced surface reflectance in the near-infrared region of the spectrum for the urban background showed the characteristic spectral shape of the water vapor absorption band, but with a lesser overall magnitude as compared to the low aerosol loading case in Figure 6. The variability of the standard deviations was of approximately the same order as that of the low aerosol loading cases in Figure 6.

c. Agricultural Background

The same five cases were covering agricultural areas in central and southern Japan were used in the differencing method. In Figure 10, the absolute average mean differenced surface reflectance in the visible end of the spectrum showed peaks of approximately 0.0015 and 0.0016 at 488 and 645 nanometers respectively. The variability was of the same order as that seen in the low aerosol regime in Figure 6. The absolute average standard deviation in the near-infrared region of the spectrum showed the expected decrease in magnitude as compared to the low aerosol loading case in Figure 6 and exhibited the spectral shape typical of the water absorption band.

D. SPATIAL RESOLUTION ANALYSIS – URBAN CASE – 27 APRIL 2001

The availability of MODIS data at 500-meter resolution for channels 1 through 7 and at 250-meter resolution for channels 1 and 2 allowed an investigation of the effects of

resolution on both the standard deviation and differencing methods. The urban background, low aerosol loading case was used for this analysis in hopes of maximizing the signal due to the high spatial variability of the urban environment. Satellite measurements at resolutions of one kilometer, 500 meters, and 250 meters were used covering the same five urban areas.

Figure 11 shows the spatial resolution analysis for the standard deviation method. Little separation is seen between the average standard deviation of surface reflectance for the three resolutions. This agreement likely results from the fact that range of surface reflectance values is the same at all three scales as are the relative proportions of the surface reflectance values to each other. Another possible explanation is that fact that the 500-meter and 250-meter data may not be sufficient to resolve urban variability any better than the one-kilometer data and no real difference is noted.

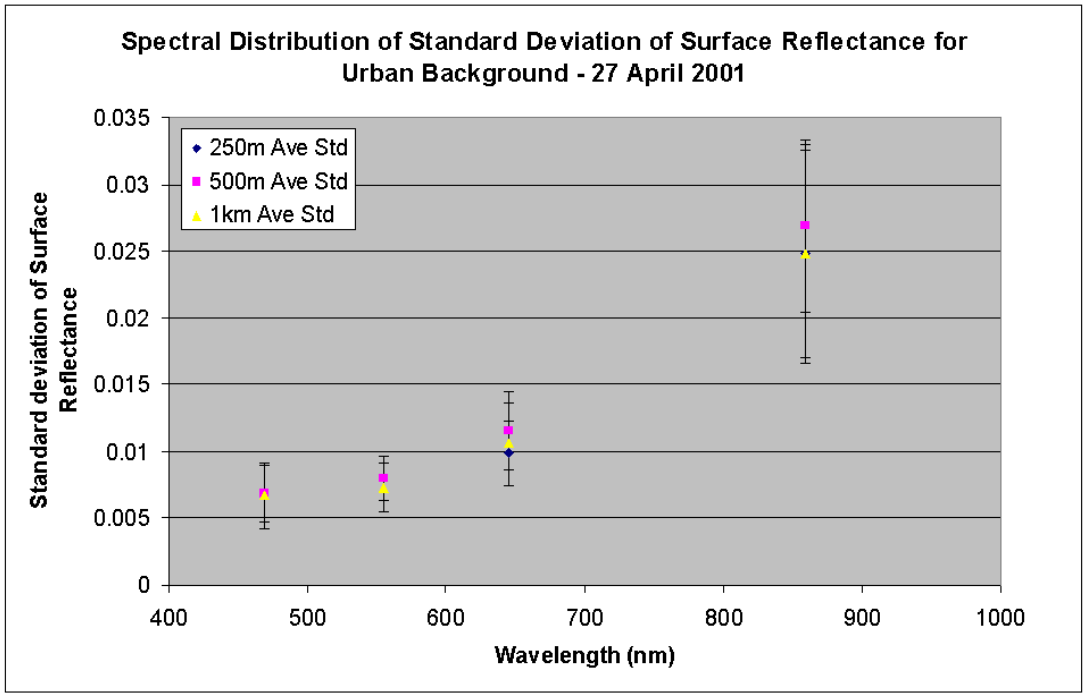

Figure 11. Spectral Distribution of Average Standard Deviation of Surface Reflectance as measured by MODIS at 1 kilometer, 500 meter, and 250 meter resolutions for the Urban Background for 27 April 2001 (Low Aerosol Loading Case).

Figure 12 shows the spatial resolution analysis for the differencing method. Figure 12 shows clear separation between the average mean differenced surface

reflectance for the three resolutions. The average mean differenced surface reflectance decreased with increased resolution. It is thought that the higher resolution data is still insufficient to resolve urban structures and therefore fails to add significant differences to the mean calculation. The higher resolution imagery displays more low contrast areas resulting in little or no pixel-to-pixel contrast and lowering the average mean differenced surface reflectance.

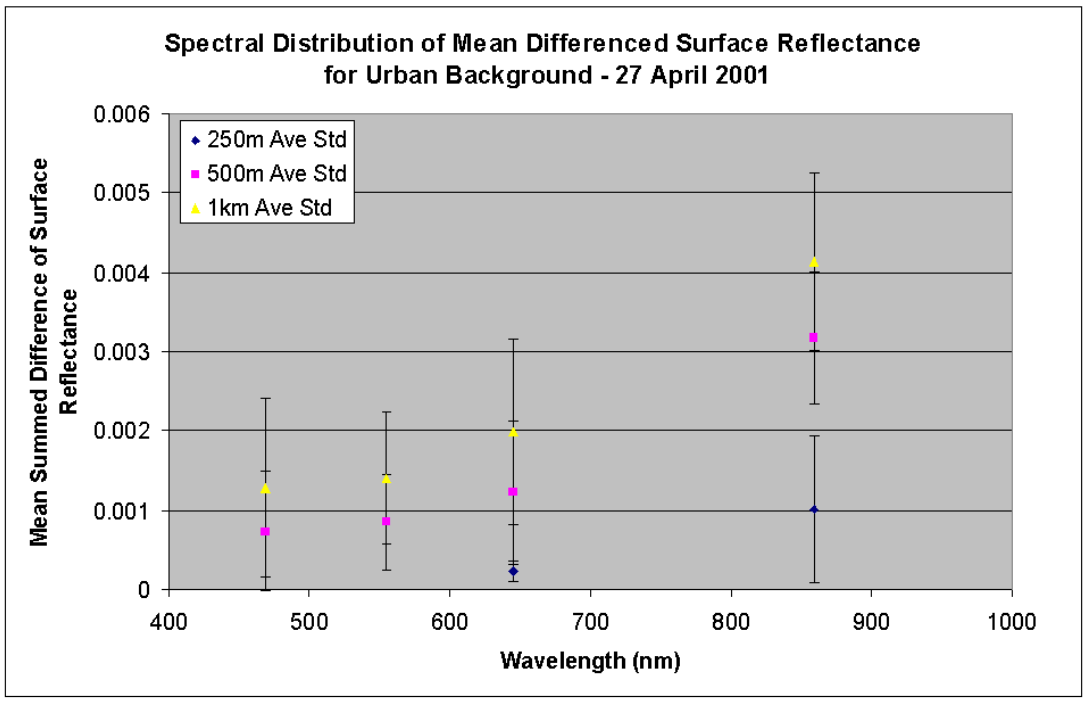

Figure 12. Spectral Distribution of Averaged Mean Differenced Surface Reflectance as measured by MODIS at 1 kilometer, 500 meter, and 250 meter resolutions for the Urban Background for 27 April 2001 (Low Aerosol Loading Case).

A separate investigation of IKONOS imagery with four channels covering the blue, green, red, and near-infrared wavelengths and a nominal resolution of one-meter, showed that extremely high resolution imagery may be better suited to detailed contrast analysis. Figure 13 shows the results of a modified standard deviation analysis and a differencing analysis over Gila Bend, Arizona. These results suggest that as resolution increases, no change or degradation in the signal may be experienced until some critical resolution threshold is reached. In Figure 13, the features of an agricultural area are easily resolved by both methods. Likewise, the features in urban settings should be

increasingly masked with increased resolution until the features can be sufficiently resolved.

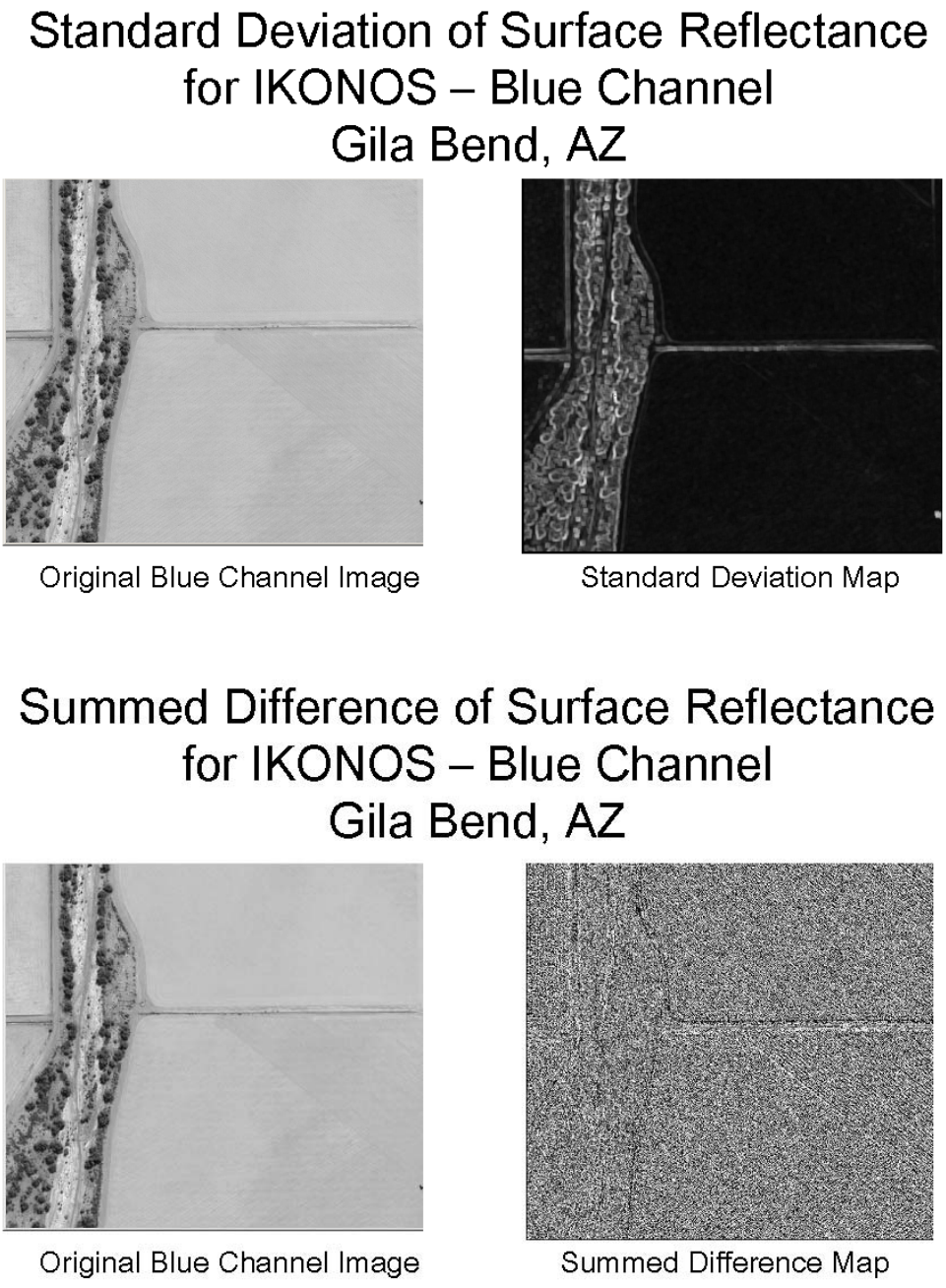

Figure 13. Examples of the Standard Deviation and Differencing Methods as used on high-resolution imagery.

THIS PAGE INTENTIONALLY LEFT BLANK

VI. CONCLUSIONS AND RECOMMENDATIONS

A. CONCLUSIONS

Two contrast reduction methods of aerosol characterization were investigated for use in surface visibility retrievals from MODIS observations. The first method used the standard deviation of surface reflectance as a measure of surface contrast. The second method used the mean of the difference in surface reflectance between adjacent pixels as a measure of surface contrast. Three different aerosol regimes over three different backgrounds in Japan were used in this investigation. The spectral distribution of standard deviation for both methods showed a unique spectral shape for each background type. The comparison of the aerosol effects within each background type showed wavelength dependence for contrast reduction based on aerosol type. Initial results of the investigation show that a surface visibility model based on contrast reduction in surface reflectance measurements from MODIS is viable.

This investigation found other environmental sensitivities beyond those to background and aerosol type mentioned above. Conservative cloud and surface water masks would be required to remove any unusually high contrast values that would lead to a high bias in retrieved visibility. A correction for sensor view angle would be required to remove a low bias for those areas near the edges of the scene. A correction for Rayleigh scattering may also be useful in retrieving more accurate surface visibilities.

The variability in each MODIS channel as measured by the standard deviation of the values from each case prevented a clear characterization of the amount of aerosol present. The temporal and spatial variability of the aerosol would require validation data of very high temporal and spatial resolution. *In situ* surface visibility and aerosol optical depth data were unavailable for the cases used in this investigation. Such data could be used to assign visibility or aerosol optical depth values to contrast measurements. The limited number of cases and the variability seen in each case would limit the statistical validity of any conclusions even if such validation data were available.

B. RECOMMENDATIONS

As a result of this study, the following recommendations are suggested:

- Repeat similar investigations over similar background types worldwide to determine uniqueness of results.

- Extend investigation to mixed aerosol regimes (e.g. dust mixed with anthropogenic pollution).

- Analyze a sufficient number of cases for each background type and aerosol regime to determine statistically significant values of average standard deviation of surface reflectance and mean differenced surface reflectance and their associated variability.

- Collect sufficient surface visibility observation data and aerosol optical depth measurements for use correlation studies of observed contrast reduction.

- Construct a surface visibility model based on the correlation between observed surface visibilities or aerosol obstacle depths and the contrast reduction as measured by the standard deviation of surface reflectance or mean differenced surface reflectance taking sensor view angle, Rayleigh scattering, the presence of clouds and surface water, background type, and aerosol type into account.

LIST OF REFERENCES

Anderson, J. R., E. E. Hardy, J. T. Roach, and R. E. Witmer, 1976: A land use and land cover classification system for use with remote sensor data. U. S. Geological Survey Professional Paper 964. 28 pp.

Andreae, M. O., R. J. Charlson, F. Bruynseels, H. Storms, R. Van Grieken, and W. Maenhaut, 1986: External mixture of sea salt, silicates, and excess sulfate in marine aerosols. *Science*, **232**, 1620-1623.

Brentzel, K., 2003: Personal Communication.

Boyd, R. W., 1988: *Radiometry and the Detection of Optical Radiation.* Wiley and Sons, 254 pp.

Charlson, R. J., S. E. Swartz, J. M. Hales, R. D. Cess, J. A. Coakley, Jr., J. E. Hansen and D. J. Hoffman, 1992: Climate forcing by anthropogenic aerosols. *Science*, **255**, 423-430.

Coakley, J. A., and P. Chylek, 1975: The two-stream approximation radiative transfer including the angle of the incident radiation. *Atmos. Sci.*, **32**, 409.

D'Almeida, G. A., P. Koepke, and E. P. Shettle, 1991: *Atmospheric Aerosol, Global Climatology and Radiative Characteristics*. A. Deepak, 561 pp.

Durkee, P. A., D. R. Jensen, E. E. Hindman, and T. H. Vonder Haar, 1986: The relationship between marine aerosol particles and satellite-derived radiance. *J. Geophys. Res.*, **91**, 4063-4072.

Durkee, P. A., F. Pfeil, E. Frost, R. Shema, 1991: Global analysis of aerosol particle characteristics. *Atmos. Environ.*, **25(A)**, 2457-2471.

Ferrare, R. A., R. S. Fraser, and Y. J. Kaufman, 1990: Satellite remote sensing of large-scale air pollution: Measurements of forest fire smoke. *J. Geophys. Res.*, **95**, 9911-9925.

Fraser, R. S., Y. J. Kaufman, and R. L. Mahoney, 1984: Satellite measurements of aerosol mass and transport. *Atmos. Environ.*, **18**, 2577-2584.

Goddard Space Flight Center, cited 2003: MODIS technical specifications. [Available online at http://modis.gsfc.nasa.gov/about/specs.html.]

Huebert, B.J., T. Bates, P.B. Russell, G. Shi, Y.J. Kim, K. Kawamura, G. Carmichael and T. Nakajima, 2003: An overview of ACE-Asia: strategies for quantifying the

relationships between Asian aerosols and their climatic impacts. *J. Geophys. Res.,* (In Press).

Intergovernmental Panel on Climate Change. *Climate Change 2001 – The Scientific Basis* (contribution of working group I to the Third Assessment Report of the Intergovernmental Panel on Climate Change). Cambridge University Press, Cambridge, 2001.

Kaufman, Y. J., 1979: Effect of the Earth's atmosphere on contrast for zenith observations. *J. Geophys. Res.*, **84**, 3165-3172.

Kaufman, Y. J., R. S. Fraser, and R. A. Ferrare, 1990: Satellite measurements of large-scale air pollution methods. *J. Geophys. Res.*, **95**, 9895-9909.

Kaufman, Y. J. and C. Sendra, 1988: Algorithm for automatic atmospheric corrections to visible and near-IR satellite imagery. *Int. J. Remote Sens.*, **9**, 1357-1381.

Kaufman, Y. J., D. Tanre, L. A. Remer, E. F. Vermote, A. Chu, and B. N. Holben, 1997a: Operational remote sensing of tropospheric aerosol over land from EOS moderate resolution imaging spectroradiometer. *J. Geophys. Res.*, **102**, 17051-17067.

Kaufman, Y. J., A. E. Wald, L. A. Remer, B.-C. Gao, R.-R. Li, and L. Flynn, 1997b: The MODIS 2.1-micrometer channel correlation with visible reflectance for use in remote sensing of aerosol. *IEEE Trans. Geosci. Remote Sens.*, **35**, 1286-1298.

Kidder, S. Q. and T. H. Vonder Haar, 1999: *Satellite Meteorology: An Introduction*. Academic Press, pp. 466.

Kiehl, J. T. and B. P. Briegleb, 1993: The relative roles of sulfate aerosols and greenhouse gases in climate forcing. *Science*, **260**, 311-314.

King, M. D., W. P. Menzel, Y. J. Kaufman, D. Tanre, B. C. Gao, S. Platnick, S. A. Ackerman, L. A. Remer, R. Pincus, and P. A. Hubanks, 2002: Cloud and aerosol properties, precipitable water, and profiles of temperature and humidity from MODIS. *IEEE Trans. Geosci. Remote Sens.*, (In Press).

Knapp, K. R. and L. L. Stowe, 2002: Evaluating the potential for retrieving aerosol optical depth over land from AVHRR Pathfinder Atmosphere data. *J. of Atmos. Sci.*, **59** (3), 279-293.

Kuciauskas, A. P., 2002: Aerosol optical depth analysis with NOAA GOES and POES in the Western Atlantic. M. S. thesis, Dept. of Meteorology, Naval Postgraduate School, Monterey, CA, 101 pp.

Mishchenko, M. K., I. V. Geogdzhayev, B. Cairns, W. B. Rossow, and A. A. Lacis, 1999: Aerosol retrievals over the ocean using channel 1 and 2 AVHRR data: A sensitivity analysis and preliminary results. *Appl. Opt.*, **38**, 7325-7341.

Morys, M. F., F. M. Mims III, and S. E. Anderson, 1996: Design, calibration and performance of MICROTOPS II hand-held ozonometer. *12th Int. Symp.on Photobiology*, Vienna, Austria, International Congress on Photobiology. [Available on line at http://www.solar.com/ftp/papers/mtops.pdf.]

Nakajima, T. and A. Higurashi, 1988: A use of two-channel radiances for an aerosol characterization from space. *Geophys. Res. Lett.*, **25**, 3815-3818.

National Aeronautical and Space Administration, cited 2003: Terra: Earth Observing System (EOS) AM-1. [Available online at http://terra.nasa.gov/Brochure/Sect_5-1.html]

Porter, J. N., M. Miller, C. Pietras, and C. Motell, 2001: Ship-based sun photometer measurements using Microtops sun photometers. *J. Atmos. Oceanic Technol.*, **18**, 765-774.

Prospero, J. M., and R. T. Nees, 1986: Impact of the North African drought and El Nino on mineral dust in the Barbados trade wind. *Nature*, **320**, 735-738.

Ramsey, R. C., 1968: *Study of the Remote Measurement of Ocean Color*. Final Report: NASW-1658. TRW, Redondo Beach, California.

Shettle, E. P., and R. W. Fenn, 1979: Models for the aerosol of the lower atmosphere and the effect of humidity variations on their optical properties. *AFGL-TR790214*, Opt. Phys. Div., Air Force Geophys. Lab., Hanscom Air Force Base, MA.

Takemura, T., T. Nakajima, O. Dubovik, B. N. Holben, and S. Kinne, 2002: Single-scattering albedo and radiative forcing of various aerosol species with a global three-dimensional model. *J. Climate*, **15**, 333-352.

Twomey, S. A., M. Piepgrass, and T. L. Wolfe, 1984: An assessment of the impact of pollution on the global albedo. *Tellus* **36B**, 356-366.

Wen, G., S. Tsay, R. F. Cahalan, and L. Oreopoulos, 1999: Path radiance technique for retrieving aerosol optical thickness over land. *J. Geophys. Res.*, 104, 31321-31332.

Whitby, K. Y., 1978: The physical characteristics of sulfur aerosols. *Atmos. Environ.*, 12, 135-159.

THIS PAGE INTENTIONALLY LEFT BLANK

INITIAL DISTRIBUTION LIST

1. Defense Technical Information Center
   Ft. Belvoir, Virginia

2. Dudley Knox Library
   Naval Postgraduate School
   Monterey, California

3. Chairman, Code MR
   Department of Meteorology
   Naval Postgraduate School
   Monterey, California

4. Professor Philip A. Durkee (Code MR/DE)
   Department of Meteorology
   Naval Postgraduate School
   Monterey, California

5. LCDR Dominick A. Vincent
   Department of Meteorology
   Naval Postgraduate School
   Monterey, California